CHEMISTRY
A EUROPEAN JOURNAL

DOI: 10.1002/chem.200902023

VIP

Efficient Homogeneous Radical-Anion Chain Reactions Initiated by Dissociative Electron Transfer to 3,3,6,6-Tetraaryl-1,2-dioxanes

Donald L. B. Stringle,[a] David C. Magri,[b] and Mark S. Workentin*[a]

Abstract: A series of 3,3,6,6-tetraaryl-1,2-dioxanes (TADs) have been investigated at an inert electrode by using cyclic voltammetry, constant potential electrolysis and digital simulations. The series consists of the phenyl-substituted TAD (**1a**), *p*-methoxy-aryl TADs (**1b**, **1c**) and the *p*-methoxy/nitro-bearing TAD (**1d**). The heterogeneous electron-transfer (ET) reduction is dissociative, causing rupture of the oxygen–oxygen bond, which generates a distonic radical-anion that reacts competitively either by β-scission fragmentation or ET. Fragmentation of the distonic radical anion yields an alkene, a substituted benzophenone, and a benzophenone radical anion. The benzophenone radical-anion propagates an efficient homogeneous ET–fragmentation chain reaction that accounts for the potential dependence of the product ratios and the low charge consumption observed in the controlled potential electrolysis experiments. Digital simulation of the experimental cyclic voltammograms allowed for estimates of the rate constants of the heterogeneous ET to the O−O bond, and for the rate constants for the β-scission fragmentation of the distonic radical-anions. Density functional theory calculations corroborate the differences in the heterogeneous kinetics of the initial dissociative ET. The endoperoxides **1a–1c** react predominantly by a concerted dissociative ET mechanism, although the data suggests a stepwise dissociative pathway is also competitive. Bearing a nitro-aryl substituent, **1d** provides a rare example of an endoperoxide that proceeds by a stepwise dissociative ET mechanism. Irrespective of the initial mechanistic details, we find a propagating radical-anion cycle is a general mechanistic feature.

Keywords: cyclic voltammetry · electron transfer · endoperoxides · fragmentation · radical ions

Introduction

Radical anions have long been recognized as an important class of reactive intermediate in synthetic organic and bioorganic chemistry.[1] They result from the transfer of a single electron to a neutral molecule to yield an intermediate possessing both a charge and radical character.[2] A long-standing misconception has been that the reactivity of radical anions, in particular for fragmentation and rearrangement reactions, could be inferred from the reactivity of analogous neutral radicals. However, a body of work by Tanko and coworkers has provided evidence that this assumption is not necessarily valid.[3–6] They demonstrated by electrochemically generating a series of cycloalkylketone radical anions that both charge and spin are governing factors in the reactivity of radical-anion rearrangements. The radical anions in these studies were observed to undergo a carbon–carbon bond fragmentation yielding a single species containing a spatially separated radical and anion, which is otherwise known as a distonic radical anion [Eq. (1)]. Recently, we provided evidence supporting these earlier findings, based on the fragmentation of distonic radical anions, which were shown to yield a localized radical-anion and a neutral molecule [Eq. (2)].[7,8]

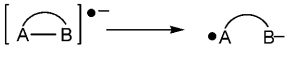

(1)

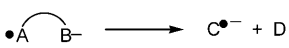

(2)

Distonic radical anions can be generated by an electron-transfer (ET) reaction to an endoperoxide.[9,10] These com-

[a] Dr. D. L. B. Stringle, Prof. M. S. Workentin
Department of Chemistry
The University of Western Ontario
London, Ontario, N6A 5B7 (Canada)
Fax: (+1) 519-661-3022
E-mail: mworkent@uwo.ca

[b] Dr. D. C. Magri
Department of Chemistry, Acadia University
Wolfville, Nova Scotia, B4P 2R6 (Canada)

Supporting information for this article is available on the WWW under http://dx.doi.org/10.1002/chem.200902023.

pounds possess an oxygen–oxygen (O–O) bond within a cyclic molecular framework. An ever increasing number of endoperoxides, many with intriguing structures and significant bioactivity, are being isolated from marine and terrestrial sources on a routine basis.[11] A high-profile example is the potent antimalarial drug, artemisinin.[12] The endoperoxides yingzhaosu C and 10,12-peroxycalamenene are unique for in addition to displaying antimalarial activity, they contain aromatic moieties.[13] Other endoperoxides with interesting molecular structures include chondrillin and muqubilin, which have been evaluated to process antitumour, antimicrobial and antiviral properties.[14] A primary aim in the study of many of these compounds has been with respect to their isolation, synthesis, and bioactivity. While considerable attention has been given to the study of artemisinin,[12] very little attention has been given, in comparison, to the relationship between the molecular structure, mechanism of action, and observed biological response of many other endoperoxides. An important consideration in the bioactivity of many of these endoperoxides is if the mechanism could be initiated by an outer-sphere dissociative-type ET reaction to the O–O bond.

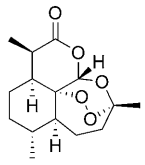

Artemisinin

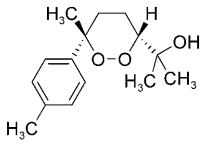

Yingzhaosu C

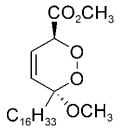

Chondrillin

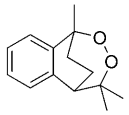

10,12-Peroxycalamenene

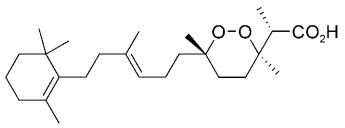

Muqubilin

Our previous studies[7,8,15–25] and those of others[26–33] have examined in detail the ET-initiated reduction mechanism of many organic peroxides and endoperoxides. These studies have provided valuable thermodynamic and kinetic information using various electrochemical techniques and application of Savéant's theory of dissociative ET.[34,35] The reduction of alkyl-substituted endoperoxides was shown to occur by a concerted dissociative ET mechanism followed by subsequent reduction and protonation as in Equations (3) and (4).[18,19] By this mechanism, ET is concomitant with O–O bond cleavage to form a distonic radical anion [Eq. (3)]. Subsequently, the alkoxyl radical portion is reduced, either heterogeneously (by an electrode) or homogeneously (by an electrochemically-generated radical-anion donor), and the alkoxides protonated to yield diol [Eq. (4)].[18,19,23]

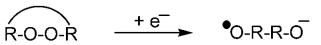

(3)

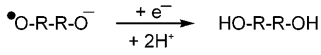

(4)

With the alkyl-substituted endoperoxides, the reactivity of the distonic radical anion was limited to reduction followed by protonation to yield the *cis*-diol in quantitative yield.[18,19] The study of 9,10-diphenyl-9,10-epidioxyanthracene (DPA-O_2) provided a glimpse into other competing reactions available to the distonic radical-anion.[22] A 1,2-phenyl (*O*-neophyl-type) rearrangement was observed to occur in competition with reduction of the oxygen-centered radical and the follow-up chemistry depended on the reduction potential of the electron donor or electrode.[23] The investigation of the ET reduction of 3,3,6,6-tetraphenyl-1,2-dioxane (TAD; **1a**) provided another reaction pathway for the distonic radical anion.[24] In our initial report, we proposed ET resulted in O–O bond cleavage generating a distonic radical anion that reacts by a β-scission fragmentation in competition with ET reduction of the oxygen-centered radical. We proposed the intermediates generated by fragmentation were responsible for initiating a homogeneous radical-anion chain reaction that accounted for the uncommon features observed in the cyclic voltammograms, notably an oxidative dip after the dissociative wave, and the pronounced potential dependence on the product ratios and low charge consumption values from the electrolysis studies.

Recently, we reported two other examples of homogeneous propagating radical-anion chain reactions initiated by dissociative ET reduction of diphenyl-substituted bicyclic endoperoxides.[7,8] Just as with **1a**, the distonic radical anion resulting from reduction of the O–O bond was observed to undergo a competing β-scission fragmentation with direct reduction from the electrode. Using various electrochemical techniques, we evaluated previously unknown kinetic and thermochemical data, delineated the reduction mechanism, and provided insight into the fragmentation chemistry of neutral biradicals and analogous distonic radical anions.[7,8]

In addition to expanding on our original study on the electrochemical reduction of **1a**,[24] we extend our discussion to include three other derivatives: the methoxy-aryl-substituted TAD **1b**, a bicyclic analogue **1c**, and the nitro/methoxy-aryl-substituted TAD **1d** (Scheme 1). We report a thorough study of the ET-initiated reduction by employing cyclic voltammetry, constant potential electrolyses, DFT calculations, and digital simulation of the experimental CVs in order to obtain a better understanding of the ET mechanism and to evaluate kinetic and thermodynamic information, in particular, the rate constant for β-scission fragmentation of the distonic radical anions. Collectively, the techniques employed allow for the evaluation of the influence aryl sub-

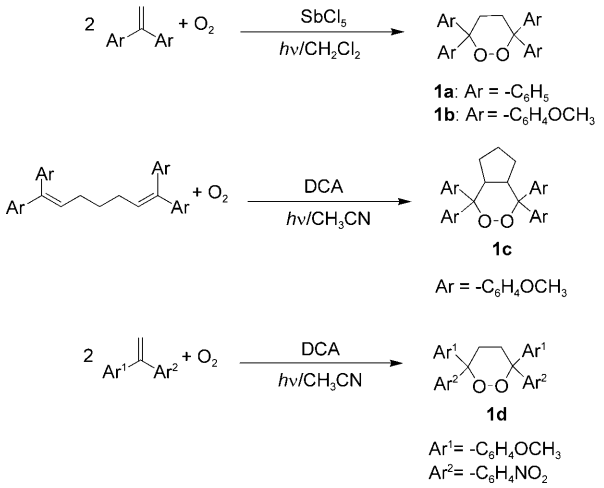

Scheme 1. Synthesis of the 3,3,6,6-tetraaryl-1,2-dioxanes from the corresponding alkene or diene ($SbCl_5$ = antimony pentachloride, DCA = 9,10-dicyanoanthracene).

stituents have on the reactivity of the distonic radical anions as well as the initial ET reduction of the O–O bond in cyclic peroxides. The phenyl and methoxyphenyl endoperoxides **1a**–**1c** react mainly by a concerted dissociative ET mechanism, although the data suggests a stepwise dissociative contribution, where as **1d** is a rare example of an endoperoxide that undergoes a solely stepwise dissociative ET mechanism.[25] Irrespective of the aryl substituent and the initial mechanistic details, we find a propagating radical-anion cycle is a general mechanistic feature.

Results and Discussion

Synthesis: The endoperoxides were synthesized by irradiating an oxygen-saturated solution of the corresponding diarylethylene (tetraarylhexadiene for **1c**) in dry dichloromethane or acetonitrile in the presence of a light-activated oxidizing agent, such as antimony pentachloride ($SbCl_5$) or 9,10-dicyanoanthracene (DCA), according to known literature methods (Scheme 1).[36–39] The alkene or diene precursors were commercially available (in the case of **1a**) or synthesized. In the final step of the syntheses, the endoperoxides precipitated out of solution and were purified by either recrystallization or column chromatography. Full experimental and characterization data are provided in the Supporting Information.

Cyclic voltammetry of 1a and 1b: The cyclic voltammetry (CV) and controlled potential electrolysis (CPE) of the TADs were studied in *N,N*-dimethylformamide (DMF) and acetonitrile (CH_3CN) with 0.10 M tetraethylammonium perchlorate (TEAP) as the supporting electrolyte at 25 °C using a 3 mm glassy carbon working electrode. Representative CVs of **1a** and **1b** are shown in Figures 1and 2 and the relevant electrochemical data are given in Table 1. As seen in Figure 1, on the initial cathodic scan of **1a**, the CV exhibits

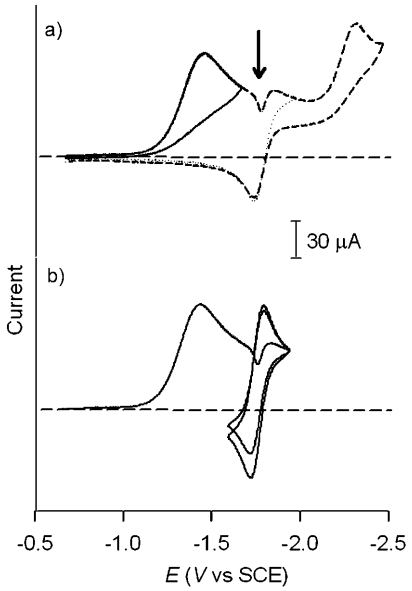

Figure 1. Cyclic voltammograms showing the reduction of a 2.2 mM solution of **1a** in 0.1 M TEAP/DMF at 0.1 $V s^{-1}$: a) scanning to −1.55 V (solid) and −1.95 V (dotted) and −2.45 V (dashed). The arrow highlights the oxidative dip (see text). b) scanning to 1.95 V and then repetitively cycling between −1.70 and −1.95 V.

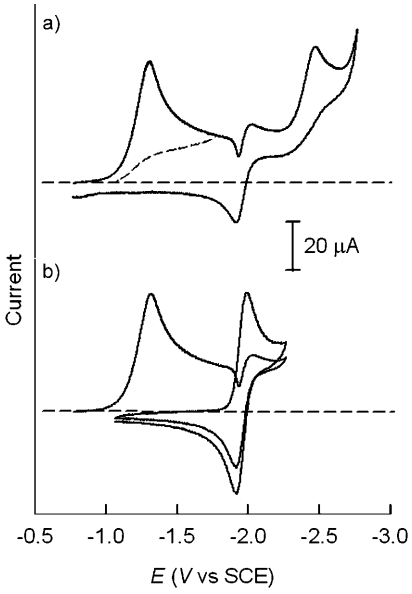

Figure 2. Representative CVs of a 1.59 mM solution of **1b** in 0.1 M TEAP/DMF at 0.1 $V s^{-1}$: a) scanning to −2.77 V (solid) and −1.77 V (dashed) and b) scanning to −2.27 V and repetitive cycling between the potential window of −1.07 to −2.27 V.

a broad, irreversible wave with a peak potential (E_p) of −1.43 V versus SCE at 0.1 $V s^{-1}$. The E_p shifts negatively by 110 mV per decade on increasing the scan rate. The peak width, defined as $|E_p - E_{p/2}|$, increases from 135 to 152 mV between 0.1 and 10 $V s^{-1}$. The transfer coefficient, α defined in Table 1, is less than 0.40, suggesting based on these criteria that the heterogeneous ET is the rate-determining step

Table 1. Cyclic voltammetry data for the TADs in DMF and CH_3CN in 0.10 M TEAP at 25 °C at a glassy carbon electrode.

	ν [V s^{-1}]	**1a**[a]		**1b**[a]		**1c**[a,b]	**1d**[c]	
E_p [V vs. SCE]	0.1	−1.43	−1.53[d]	−1.29	−1.36[d]	−1.80	−0.918	−0.887[d]
	1.0	−1.52	−1.65[d]	−1.39	−1.48[d]	nd[e]	−0.914	nd[d,e]
	10	−1.64	−1.78[d]	−1.50	−1.60[d]	nd[e]	−0.953	nd[d,e]
$\Delta E_{p/2} = \lvert E_{p/2} - E_p \rvert$ [mV]	0.1	135	152[d]	98	121[d]	223	76	82[d]
	1.0	144	174[d]	105	145[d]	nd[e]	64	nd[d,e]
	10	152	197[d]	127	172[d]	nd[e]	58	nd[d,e]
$I_p/C\nu^{1/2}$ [μA s$^{1/2}$ V$^{-1/2}$ mM^{-1}][f]		25	24[d]	39	31[d]	24	40	81[d]
$\alpha = 1.857RT/F\Delta E_{p/2}$	0.1	0.35	0.31[d]	0.49	0.39[d]	0.21	0.63	0.58[d]
	1.0	0.33	0.27[d]	0.45	0.33[d]	nd[e]	0.74	nd[d,e]
	10	0.31	0.24[d]	0.37	0.28[d]	nd[e]	0.82	nd[d,e]
α[g]		0.26	0.22[d]	0.28	0.22[d]	0.28	0.87	0.49[d]
$\partial E_p/\partial(\log \nu)$ [V]		−0.11	−0.13[d]	−0.11	−0.12[d]	−0.10	−0.03	−0.06[d]

[a] CVs in DMF/0.10 M TEAP. [b] CVs in acid display two amalgamated waves, initial peak potential obscured at all scan rates. [c] CVs in CH_3CN/0.10 M TEAP; CVs in DMF with and without acid were unreliable. [d] In the presence of excess weak acid the initial wave becomes completely irreversible. [e] Peak obscured by following wave; unable to determine peak potential; nd = not determined. [f] Peak current normalized for concentration and scan rate. [g] $\alpha = 1.15RT/F(dE_p/d\log \nu)$.

by a concerted dissociative mechanism (vide infra).[34] At all scan rates examined, the initial peak remains irreversible. The CVs of **1b** are similar to those of **1a** in most respects. A noticeable difference is that the initial cathodic peak of **1b** is considerably sharper with the $\Delta E_{p/2}$ increasing from 98 mV at 0.1 V s^{-1} to 127 mV at 10 V s^{-1}. The E_p is located at −1.29 V versus SCE at 0.1 V s^{-1}, and also shifts negatively by 110 mV per decade with increasing scan rate.

Scanning in the cathodic direction beyond the initial wave, both **1a** and **1b** exhibit a sharp, oxidative current dip at lower scan rates about −1.8 V. This dip becomes less pronounced with increasing scan rates ultimately disappearing at scan rates over 1.0 V s^{-1}.[7,8] The current dip directly precedes the reversible wave of the product resulting from the initial ET reduction step. By repetitive cycling voltammetry (Figures 1b and 2b), the standard reduction potentials of the redox couples were determined to be $E^o = -1.77$ and −1.95 V versus SCE from the CVs of **1a** and **1b**, respectively. These reversible waves are due to the reduction of benzophenone (**4a**) and 4,4′-dimethoxy benzophenone (**4b**) to the radical anions **5a** and **5b**, respectively, as verified by comparison with authentic samples. Following the reversible redox couple in each CV is an irreversible reduction wave (with $E_p = -2.40$ and −2.45 V vs. SCE) in the CVs of **1a** and **1b**, which are due to the reduction of the corresponding benzophenone radical-anion to its dianion as confirmed from the CVs of authentic **4a** and **4b**, respectively.

Cyclic voltammetry of 1c: Cyclic voltammograms of **1c** are shown in Figure 3. A broad, irreversible dissociative wave is located at a $E_p = -1.80$ V versus SCE at 0.1 V s^{-1}. The peak is observed to shift negatively by 100 mV per decade over a scan rate range of two log decades. The dissociative wave is followed by a current oxidative dip that precedes the reversible wave due to the reduction of **4c**, which is apparent from the repetitive cycling experiments. At higher scan rates, the dissociative wave converges with the **4c** reduction peak, rendering the measurement of the E_p intractable above 1.0 V s^{-1}. Scanning to more negative potentials beyond the redox couple of **4c** reveals the irreversible wave due to the reduction of **4c** to its dianion.

Some differences between the CVs of **1a** and **1c** are worthy of further mention. At scan rates where the peak potential is observed, the E_p for **1c** occurs at much more negative potentials than for either **1a** or **1b**. The peak heights of **1c** are also much lower than the peak heights of its monocyclic analogues **1b** and characterization of the dissociative wave of **1c** is hindered by the close proximity of the reversible wave **4c**, which also contributes to the smaller peak height. Precautions were taken to ensure that the differences between the CVs of **1b** and **1c** were real and not due to adsorption effects on the electrode. As we will discuss in greater detail, digital simulation of the experimental voltammograms provides evidence that these divergences are correlated to differences in the heterogeneous reduction kinetics.

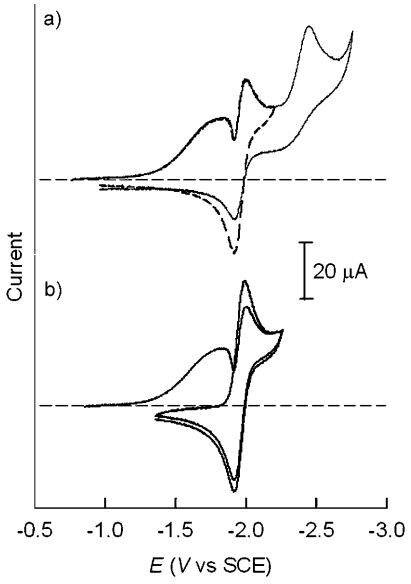

Figure 3. Representative CVs of a 1.50 mM solution of **1c** in 0.1 M TEAP/DMF at 0.1 V s^{-1}: a) scanning to −2.76 V (solid) and −2.21 V (dashed) and b) scanning to −2.21 V and repetitively cycling between a potential window of −1.36 and −2.21 V.

Cyclic voltammetry of 1d: For the TADs **1a**–**1c**, the dissociative peak shape and the variations of peak breadth and

height are suggestive of some degree of a concerted dissociative process in which heterogeneous ET and O–O bond cleavage occur simultaneously. However, the voltammetry of **1d** is intriguing in that a broad, irreversible peak is not evident at any examined scan rate. Figure 4 shows representative CVs of **1d** in CH_3CN rather than in DMF as the CVs were not readily reproducible. At lower scan rates, a shoulder is observed on the initial wave at about −0.8 V, which we interpret as the beginning of the dissociative wave. As the scan rate is raised, the dissociative wave blends into the reversible couple, which is assigned to the ET reduction of 4-methoxy-4′-nitrobenzophenone (**4d**). The CV of **4d** in CH_3CN replicates most of the CV features of **1d**. For example, **4d** exhibits two reversible reduction waves with $E^{o}_{R1} = -0.87$ V and $E^{o}_{R2} = -1.32$ V versus SCE. In the CVs of **1d**, a small peak between the two redox couples, as indicated by the arrow in Figure 4a, is attributed to the reduction of 1,4-*bis*(4-methoxyphenyl)-1,4-*bis*(4-nitrophenyl)butane-1,4-diol (**3d**). This assignment is based on the voltammetry of 4-methoxy-4′-nitrobenzhydrol, which displays similar voltammetry characteristics to the middle peak at −1.2 V in the CVs of **1d**. Further support for this assignment is obtained from the controlled potential electrolysis experiments.

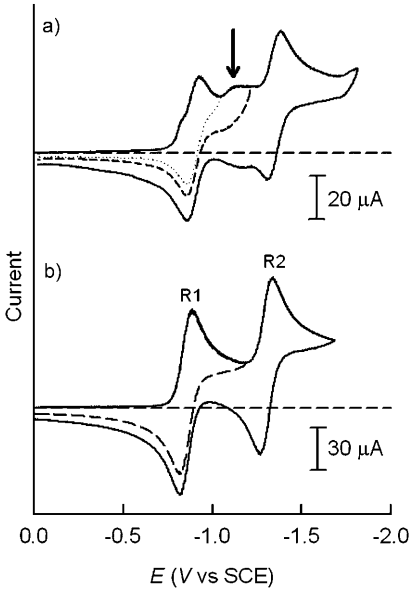

Figure 4. Representative CVs for **1d** and **4d** in 0.1 M TEAP/CH_3CN when scanning at 0.1 $V s^{-1}$: a) 1.2 mM **1d** scanning to −1.05 V (dotted), −1.22 V (dashed) and −1.82 V (solid). The arrow indicates the reduction peak assigned to **3d** (see text). b) 2.4 mM **4d** scanning to −1.19 V (dashed) and −1.69 V (solid).

Controlled potential electrolyses (CPE): CPE experiments with **1a**, **1b**, and **1d** were performed in dimethylformamide (DMF) and acetonitrile (CH_3CN) with the aim of producing sufficient quantities of the reduction products for isolation, identification, and quantification. The results of the CPE experiments are contained in Table 2and the structures of the products are shown in Scheme 2. The data show the product ratios are dependent on the applied potential during the electrolyses and the presence of a weak acid. Electrolyses of **1a** at a potential near its E_p in DMF and CH_3CN yields 1,1,4,4-tetraphenyl-1,4-butanediol (**3a**) in a 89:11 ratio over benzophenone (**4a**). Similarly, reducing **1b** at its E_p produ-

Table 2. Product ratios and charge consumption data obtained from the controlled potential electrolysis of TADs in DMF and CH_3CN in presence of 0.10 M TEAP at a rotating disk electrode with a 12 mm glassy carbon tip.

Endoperoxide	Electrolysis potential[a]	Solvent	Product ratio (**3**:**4**)	n[f]
1a	E_p	DMF	89:11[c]	1.9
1a	$< E^{o}_{4a/5a}$	DMF	2:98[c]	0.08
1a	$< E^{o}_{4a/5a}$	DMF[b]	99:1[c]	2.0
1a	E_p	CH_3CN	89:11[c]	1.9
1a	$< E^{o}_{4a/5a}$	CH_3CN	46:54[c]	0.4
1a	$< E^{o}_{4a/5a}$	CH_3CN[b]	97:3[c]	1.9
1b	E_p	DMF	>100:1[d]	1.9
1b	$< E^{o}_{4b/5b}$	DMF	3:97[d]	0.2
1b	E_p	CH_3CN	>100:1[d]	1.9
1b	$< E^{o}_{4b/5b}$	CH_3CN	3:97[d]	0.08
1d	E_p	CH_3CN	9:91[e]	0.3
1d	E_p	CH_3CN[b]	78:22[e]	2.0

[a] $E^{o}_{4a/5a} = -1.77$, $E^{o}_{4b/5b} = -1.95$ V vs. SCE. [b] In the presence of 20 mM 2,2,2-trifluoroethanol.[c] Determined by GC. [d] Determined by HPLC. [e] Determined by ^1H NMR spectrum integration. **3** = diol, **4** = benzophone, **5** = benzophenone radical anion. [f] Number of electron equivalents consumed during electrolysis in $F mol^{-1}$.

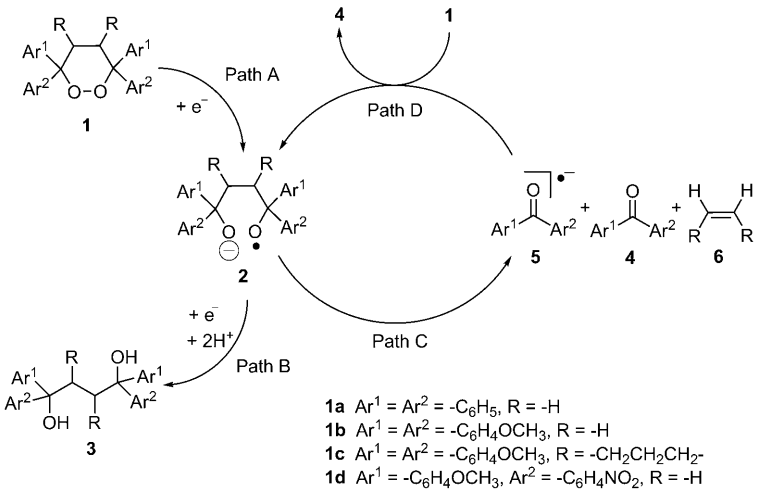

Scheme 2. The catalytic radical-anion chain mechanism proposed for the 3,3,6,6-tetraaryl-1,2-dioxanes **1a**–**1d**.

ces 1,1,4,4-(4-methoxyphenyl)-1,4-butanediol (**3b**) in near quantitative amount with only a trace amount of 4,4′-dimethoxybenzophenone (**4b**) in the product mixture. In both cases, nearly two electron equivalents of charge are required for complete reduction of the endoperoxides.

However, when the applied potential is set negative to the standard potential of the benzophenone species $E^{o}_{4/5}$ (e.g., $E^{o} = -1.77$ and -1.95 V versus SCE), the product ratios are inverted. Under these conditions in DMF, the benzophenone compound is the primary product in greater than 96% with little diol formed.

Most significantly, at an applied potential negative to $E^{o}_{4/5}$, no more than 0.4, and as little as 0.08, electrons per molecule are needed for complete conversion of starting material to products. In contrast, the results from the CPE experiments of **1d** are quite different than those of **1a** and **1b**. CPE of **1d** at the foot of the reduction wave results in formation of benzophenone in a ratio of 91:9 over diol with a modest charge consumption of 0.3 F mol^{-1}. This is counterintuitive based on the observations from **1a** and **1b.**

Electrolysis experiments of **1a** and **1d** were also carried out in the presence of 2,2,2-trifluoroethanol (TFE) and the results of these experiments are also summarized in Table 2. CPE of **1d** in CH_3CN in the presence of excess TFE at an applied $E = -0.90$ V yields predominantly diol **3d**, but with a significant amount of benzophenone **4d** with a charge consumption of 2 F mol^{-1}. The product ratio by ^{1}H NMR spectroscopy was a 4:1 ratio of **3d** over **4d**.[40] From the results in Table 2, it can be generalized that the presence of an acid results in an increased amount of diol.

Reaction mechanisms of 1a–1c: Our proposed reaction mechanism for **1a–1c**, illustrated in Scheme 2, accounts for the observed voltammetry, the isolated products, the potential dependence of the product ratios, and the charge consumption. It consists of four main steps. The first step (labeled path A) is the initial ET to the endoperoxide, which occurs by a dissociative mechanism resulting in cleavage of the O–O bond to generate the distonic radical anion **2**. Reduction of the alkoxy radical center of **2** to yield the dianion, followed by protonation results in the diol **3** (through path B).[41] In competition with reduction of **2**, β-scission fragmentation results in the corresponding benzophenone **4**, its radical anion **5**, and an alkene **6** (path C). The production of **5** is the crucial step in the propagating radical-anion chain mechanism. Since the standard potential of **4a** ($E^{o}_{4a/5a}$) is over 30 mV negative with respect to the E_p of **1a**, and $E^{o}_{4b/5b}$ is over 60 mV negative with respect to the E_p of **1b**, ET from **5a** to **1a** and **5b** to **1b** are both thermodynamically favorable processes. Hence, the fourth and final step in Scheme 2 is the homogeneous reduction of **1** by **5** to generate **4** and another species of **2** (path D). The isolation of **4a** and **4b** from the reduction of **1a** and **1b**, respectively, supports β-scission fragmentation of **2** as a competitive pathway. In fact, considering that **2** is produced near the electrode surface, the fragmentation must occur rapidly in order to compete with reduction. When the electrode potential is negative with respect to $E^{o}_{4/5}$, any **4** produced by fragmentation of **2** is reduced to its anion, **5**. This is a key aspect in the mechanism. At these negative potentials, for every distonic radical anion that undergoes fragmentation, two equivalents of **5** are generated, one directly from the β-scission fragmentation and the other indirectly from the single heterogeneous ET reduction of **4**. This results in a substantial concentration of **5** in the vicinity of the electrode surface. As more **1** diffuses toward the electrode, the endoperoxide is intercepted by **5** and is reduced homogeneously rather than heterogeneously at the electrode surface. This triggers the propagating ET radical-anion chain reaction. As species **2** is formed further and further away from the electrode surface, heterogeneous ET reduction cannot as readily compete due to the exponential distance dependence on the ET so that fragmentation (path C) becomes favored over reduction (path B). As a consequence, the homogeneous reduction of **1** by **5** produces more **2**, which generates at least another equivalent of **5**. Therefore, at $< E^{o}_{4a/5a}$, the charge necessary for complete reduction of **1** is the amount needed to generate enough **5** near the electrode surface to initiate the fragmentation-homogeneous ET radical-anion chain process. Once initiated, the chain reaction spreads into the bulk solution and consumes the rest of **1** without requiring additional charge. Hence the low charge consumption values ranging from 0.4 to 0.08 F mol^{-1}.

At potentials corresponding to the E_p, which is positive to the $E^{o}_{4a/5a}$, the radical-anion propagating chain mechanism still operates, but it is not charge efficient. The charge consumption is stoichiometric, rather than catalytic, as nearly 2 F mol^{-1} of charge is required at these potentials. Products resulting from fragmentation are observed, but to a much lesser extent. In this instance, only one equivalent of **5** is possible from each fragmentation event, as **4** cannot be directly reduced by the electrode. Thus, the amount of **4** at the electrode interface does not readily accumulate, and hence, the concentration of **4** is much lower such that the bimolecular reduction **1** and **2** is no longer as competitive as the heterogeneous ET reduction.

The proposed mechanism also accounts for the oxidative current dip observed in the voltammetry of **1a–1c**, as indicated by the arrow in Figure 1. The value of the current is representative of the concentration of the electroactive species **5** present at the electrode surface. The dip occurs at potentials at which an equilibrium exists between **4** and **5**. As the concentration of **5** near the electrode increases, we see a dramatic drop in current as a result of there being less **1** to reduce at the electrode. The rapid, sudden drop in current reflects the amount of **1** that is not reaching the electrode, and instead being reduced homogeneously by **5**, as a result of the radical-anion chain process.

As mentioned earlier, the presence of excess weak acid has a significant effect on the product yields. According to Scheme 2, acid could suppress the homogeneous propagating mechanism in two ways. First, acid could protonate the distonic radical anion **2**. In the presence of excess TFE, an almost quantitative amount of diol was isolated in the CPE

experiments of **1a** in comparison to only 89% in the absence of acid. The presence of acid causes a loss in chain reactivity due to the protonation of **2**, which yields the alkoxyl radical species **2aH**. Under these circumstances, the fragmentation of **2aH** could produce benzophenone, ethylene, and a diphenylhydroxymethyl radical. None of these fragments are capable of acting as a homogeneous ET donor to reduce **1a**, so the chain process ceases to operate efficiently. The second way excess acid could potentially affect the reduction mechanism is by protonating the benzophenone radical anion to yield a ketyl radical intermediate, which on further reduction and protonation would result in benzhydrol. This second possibility results if the β-scission fragmentation of **2aH** is competitive with electrode reduction. In our experiments, no benzhydrol was detected from the CPE of **1a** in the presence of excess TFE. The experimental evidence suggests excess weak acid favors protonation of **2**, which hinders the β-scission fragmentation and favors the formation of **3** by path B, thus inhibiting the radical-anion chain reaction through path C. This interpretation is consistent with our previous studies that the fragmentation rates of distonic radical anions are different from the analogous radical species.[7,8]

Reaction mechanism of 1d: Figure 4 highlights the lack of a broad and irreversible wave normally associated with ET reduction of an endoperoxide. Rather, the dissociative wave of **1d** at −0.8 V is the small shoulder in Figure 4, on the left side of initial reversible redox couple due to the reduction of the nitrobenzene units. Unlike the CVs for the other three endoperoxides, the E_p of **1d** occurs very close to the reduction potential of the benzophenone **4d** ($E^{o}_{\mathbf{4d/5d}}$), whereas the reduction potentials of **4a–4c** are significantly negative with respect to the dissociative waves of **1a–1c**. The consequence is that the reduction of **1d** essentially occurs under conditions that induces the homogeneous ET-fragmentation radical-anion chain reaction from the onset. As soon as **1d** is reduced at the electrode, the homogeneous reduction very rapidly dominates the heterogeneous ET reduction. In the case of **1a–1c**, the homogeneous ET donor is the radical anion **5a–5c**. However, the inclusion of the nitro substituent in **1d** facilitates the formation of a number of products and intermediates potentially capable of also behaving as homogeneous ET donors including the diol **3d**.

Digital simulations of the cyclic voltammograms: The CVs of the four TADs were simulated using Digisim 3.0 software. The mechanism employed to simulate the cyclic voltammograms and to determine unknown kinetic and thermodymanic information is based on Scheme 2. A summary of the most influential elementary steps included in the simulations are shown in Scheme 3. In both the concerted and stepwise

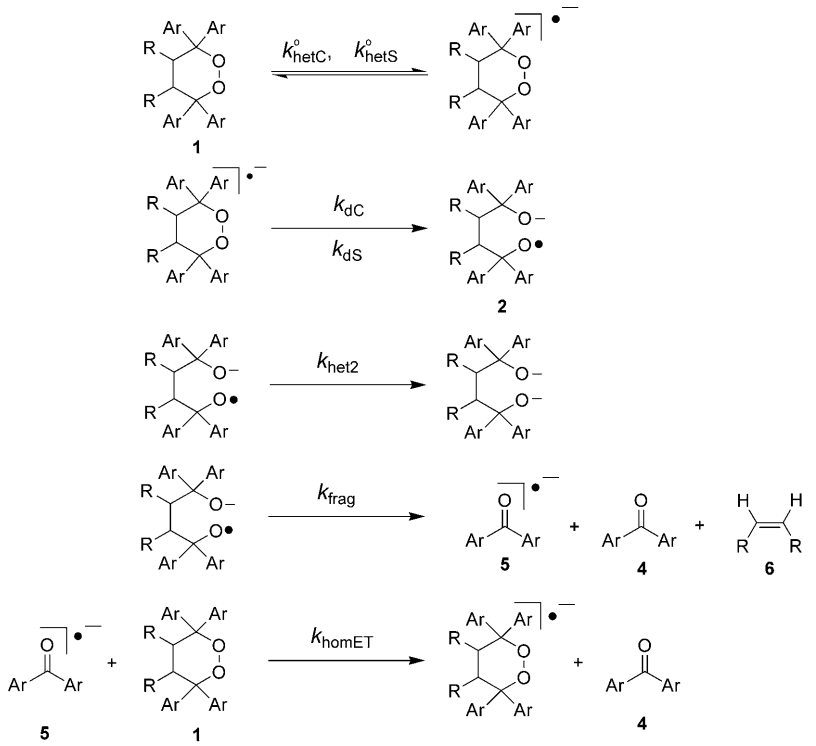

Scheme 3. A summary of the most influential elementary steps in the digital simulations of the 3,3,6,6-tetraaryl-1,2-dioxanes **1a–1d**. Refer to Scheme 2 for substituents key for Ar and R.

mechanisms, there are at least five rate constants of pertinence: 1) the heterogeneous ET to the O–O k^{o}_{hetC} or k^{o}_{hetS}; 2) fragmentation of the O–O bond k_{dC}, or k_{dS}; 3) the heterogeneous ET to the distonic radical-anion, k_{het2}; 4) the β-scission fragmentation of **2**, k_{frag}; and 5) the homogeneous reduction of **1** from **5** k_{homET}. The parameters resulting from the simulations are reported in Table 3. Initial input values for many of the parameters, including the standard potential E^{o}_{C}, the heterogeneous rate constants k^{o}_{hetC} and the diffusion coefficient D were taken from reported values.[17,23,26] Traditionally, this information has been conveniently attained by convolution potential sweep voltammetry (CPSV).[35a,42] However, the non-Cottrell behavior (i.e., the oxidative dip) in the voltammetry due to the homogeneous ET–fragmentation cycle hindered the quality of the data, even in the presence of excess weak acid. Notably, the convoluted curves

Table 3. Key parameters for the heterogeneous and homogeneous ET reduction as determined by digital simulation of the cyclic voltammograms.[a,b]

Parameters	**1a**	**1b**	**1c**	**1d**
E^o_C [V]	−0.96	−1.15	−0.89	n/a[c]
k^o_{hetC} [cm s^{-1}]	2.4×10^{-6}	4.2×10^{-4}	4.7×10^{-8}	n/a[c]
λ+BDE, [V]	1.2	1.2	1.1	n/a[c]
E^o_S [V]	n/a[c]	−1.15[d]	n/a[c]	-1.05[d]
k^o_{hetS} [cm s^{-1}]	n/a[c]	3.5×10^{-4}[d]	n/a[c]	0.1[d]
α	n/a[c]	0.45[d]	n/a[c]	0.4[d]
k_{dC} [s^{-1}]	1×10^{13}	1×10^{13}	1×10^{13}	n/a[c]
k_{dS} [s^{-1}]	n/a[c]	1×10^{13}	n/a[c]	1×10^{8}
E^o_2 [V]		−0.1		
k^o_{het2} [cm s^{-1}]		0.1		
k_{homET} [M^{-1} s^{-1}]	3.7×10^{5}	3.5×10^{6}	1.5×10^{6}	7.3×10^{5}
k_{frag} [s^{-1}]	1.4×10^{6}	1.1×10^{6}	8.3×10^{6}	4.9×10^{4}
D [cm^2 s^{-1}]	5.3×10^{-6}	4.8×10^{-6}	4.4×10^{-6}	1×10^{-6}

[a] The subscripts C and S identify parameters specific to a concerted dissociative and stepwise dissociative ET reaction, respectively. [b] Listed values are averages from many simulations at various scan rates. [c] n/a = not applicable. [d] Simulations employed Butler–Volmer electrode kinetics for initial ET.

were found to be unreliable as the limiting current was not scan-rate independent and a constant plateau current was not obtained. Therefore, average values were initially taken from bicyclic endoperoxide CPSV studies; for example, the E^o_C range from −0.6 to −1.2 V, k^o_{hetC} and D average 6×10^{-7} and 6×10^{-6} cm^2 s^{-1}.[7,8,23] Approximately constant values of 1.2 V, 0.1 V, and 0.1 cm s^{-1} were used for the BDE+λ, E^o_2, and k^o_{het2}, the last two parameters being specific to the heterogeneous reduction of the distonic radical anion.

Examples of high-quality reproductions of the CVs of **1a**–**1d** can be found in Figure 5 overlapping the experimental CVs at a scan rate 0.1 V s^{-1} and the simulation parameters

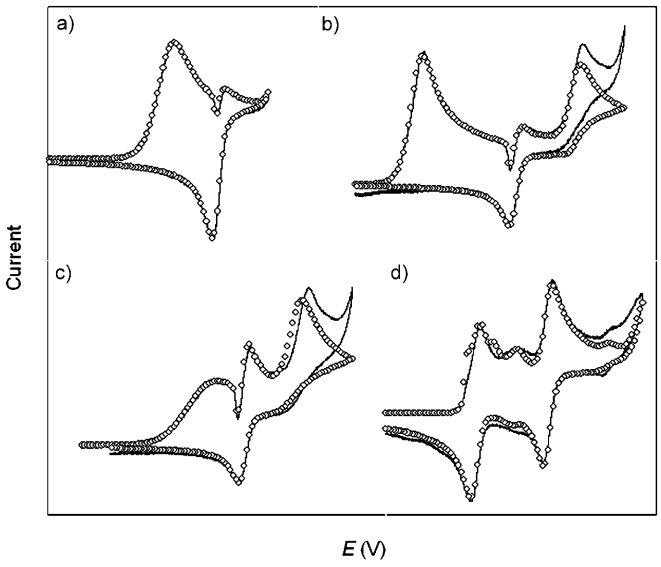

Figure 5. Comparison of simulated CVs (circles) with the experimental CVs (line) at 0.1 V s^{-1}: a) a 1.95 mM solution of **1a** in 0.1 M TEAP/DMF; b) a 1.59 mM solution of **1b** in 0.1 M TEAP/DMF; c) a 1.50 mM solution of **1c** in 0.1 M TEAP/DMF; and d) a 1.13 mM solution of **1d** in 0.1 M TEAP/CH_3CN.

can be found in Table 3. In these simulations, emphasis was placed on achieving parameter constants that provided precise simulations at a range of scan rates from 0.1 to 10 V s^{-1}. Prudence was placed, in particular, on accurately simulating the peak current at all scan rates investigated. Simulations were also done at two or more concentrations for each TAD.

Overall, the differences in the parameters for **1a**–**1c** are rather subtle with the exception of the k^o_{hetC} values. There is a 10000-fold difference in the rate constants between **1b** and **1c**, which is attributed to the more rigid structure of **1c.** The k^o_{hetC} for **1a** is in the middle of the range with a value of 2.4×10^{-6} cm s^{-1}. The diffusion coefficients decrease slightly from 5.3×10^{-6} for **1a** to 4.4×10^{-6} cm^2 s^{-1} for **1c** in keeping with the increasing sweep radius.

A primary objective of the simulations was to obtain rate constants for the β-scission fragmentation k_{frag} and for the homogeneous ET to the endoperoxide k_{homET}. The value of k_{homET} was determined from simulation of the observed oxidative dip. It was found that the shape of the dip was highly sensitive to k_{homET}, and thus used as a diagnostic parameter in the simulations. The driving force for the homogeneous ET reduction of **5a** to **1a** is calculated to be approximately −17 kcal mol^{-1}. The homogeneous ET between **5d** and **1d** is not expected to follow the same activation-driving force relationship as for other peroxides, as it is a stepwise reduction.

The ET reduction of **1d** clearly occurs by a stepwise dissociative mechanism. The E^o value for reduction of **1d** was estimated based on the E^o determined for 4-methoxy-4′-nitrobenzhydrol (−1.1 V vs. SCE), which served as a reasonable model. The E^o value assigned to **1d** is more negative than the E^o of **4d**, because the additional electron of its radical anion **5d** can be delocalized onto the carbonyl moiety. This effect is seen in the E^o values of nitrobenzene (−1.12 V vs. SCE) and *tert*-butyl 4-nitrobenzoate (−0.89 V vs. SCE), in which the ester function located *para* to the nitro group results in a significant decrease in the E^o through the enhanced stabilization of the radical anion.

The initial heterogeneous ET to **1d** has a rate constant of 0.1 cm s^{-1}. This value is much larger than the rate constants for the concerted mechanisms for **1a**–**1c**, which have values smaller than 10^{-3} cm s^{-1}. In addition, the rate constant for dissociation of the O−O radical anion is 1×10^{8} s^{-1}, which is five orders of magnitude lower than for the concerted mechanism. Another indication that the reduction mechanism for **1d** is indeed stepwise dissociative is the fact that the CVs shift by only 30 mV per tenfold increase in scan rate.

For comparison, simulations of **1d** were also carried out assuming a concerted dissociative ET mechanism. The same E^o value as for **1a** was used, as the electron-withdrawing effect of the nitro–aryl groups on the O−O bond is expected to offset the electron-donating effect of the methoxy–aryl groups. The k^o_{het} value was taken from the results employed in the simulations of **1b**, which has equatorial 4-methoxyphenyl rings similar to **1d**. At 0.1 V s^{-1}, the simulation was found to be similar as in the stepwise mechanism; however,

with increasing scan rate, the initial peak becomes broader and shifts increasingly to more negative potentials in excess of 60 mV per log decade, thus ruling out a purely concerted mechanism.

The fragmentation rate constants for the distonic radical anions from the digital simulations range from 10^4 to 10^6 s^{-1}. Our estimates for bicyclic diphenyl-substituted endoperoxides had a lower limit of 3×10^7 s^{-1}.[7,8] A possible explanation for the difference may be due to the conformation of the distonic radical anion upon O–O bond cleavage. The bicyclic diphenyl-substituted endoperoxides are anticipated to be in a strained conformation with the lone pairs on the oxygen atoms eclipsing one another. Cleavage of the O–O relieves strain energy and facilitates the β-scission fragmentation. In contrast, the TAD endoperoxides **1a**–**1d** are probably in a chair conformation upon rupture of the O–O bond, so that there is a lesser degree of strain. Furthermore, in a chair conformation the electron lone pairs are staggered so there is also a lesser degree of charge repulsion than associated within bicyclic endoperoxides.

Laser flash photolysis of **1a** provided a lower limit for the rate constant of fragmentation of the biradical from homolytic O–O bond cleavage. The transient spectrum showed only the decay of triplet benzophenone. Given that the laser pulse is 20 ns suggests that β-scission fragmentation of the dialkoxy radical to benzophenone occurs with a rate constant of at least 10^8 s^{-1}. Previous studies from the photolysis and thermolysis of 3,3,6,6-tetramethyl-1,2-dioxanes have suggested a concerted fragmentation process.[43] The impact of the additional charge on the distonic radical anion **2a** is significant, compared to its biradical analogue, as it results in a 100-fold decrease in the rate of fragmentation of the charged intermediate. Discrepancies between the rates constants for fragmentation of radical-anions and their neutral radical counterparts are only recently becoming known.[3,4,7,8] For the fragmentation of **2a**, it is suggested that the alkoxyl anion is more readily stabilized by the aryl rings than the alkoxyl radical center. This assessment agrees with the trend in the fragmentation rate constants as **2d** has the lowest value as the 4-nitrophenyl rings provide the greatest stabilizing effect on the alkoxide anion.

Density functional theory calculations: In the digital simulations, we used a value of 1.2 V or 27.7 kcal mol^{-1} for the sum of BDE$+\lambda$. These values correspond to an intrinsic barrier of 6.9 kcal mol^{-1} (divided by 4). Assuming a concerted dissociative ET mechanism for **1a**, a simple arithmetic calculation yields a BDE of 17.7 kcal mol^{-1}, if the lowest estimated value for λ is 10 kcal mol^{-1}.[7,8,19] Our studies on the heterogeneous ET of bicyclic diphenylendoperoxides has consistently resulted in intrinsic barriers about 10 kcal mol^{-1}, which we previously attribute to a concerted ET mechanism involving cleavage of a weak O–O bond.[7,8] Although a lower limit of 18 kcal mol^{-1} for the BDE is in line with previous studies, the λ value in these studies was estimated to be 20 kcal mol^{-1}. This difference in the λ values may be reconciled, but only partly, by considering the conformation of the endoperoxide on acceptance of the incoming electron. The endoperoxides **1a**–**1d** are already in a chair conformation on accepting the electron, in contrast to the bicyclic diphenylendoperoxides, which are initially in a rigid, boat conformation with the lone pairs on the oxygen atoms eclipsing. Hence, a greater reorganization energy should be expected for the [2,2,1] and [2,2,2]bicyclic endoperoxides.

Additional insight into the reasons for the low intrinsic barrier for **1a**–**1d** comes from recent studies on the ET reduction of diaryl disulfides.[44,45] In these studies, the authors suggested the ET proceeds by a mechanism somewhere between the two mechanistic extremes of stepwise and concerted. Notably, the $\Delta G_o^{\neq}$ was found to be too large for a typical stepwise process, and upon investigation it was concluded that there is a significant contribution from S–S bond lengthening to the radical anion. In hindsight, a related situation may have been serendipitously observed during the ET reduction of DPA-O_2, in which the $\Delta G_o^{\neq}$ was lower than expected for a purely concerted ET mechanism.[23] The lower values for the $\Delta G_o^{\neq}$ of **1a**–**1d**, although admittedly puzzling to us at first, lead us to consider a competitive concerted–stepwise ET dichotomy.

To investigate our hypothesis we employed DFT calculations. The calculations involved a geometry optimization of the TAD structure by using semi-empirical PM3 calculations followed by a single-point energy DFT calculation using the B3LYP//6-31G** basis set to calculate the LUMO. A depiction of the calculated LUMOs for **1a**, **1b**, and **1d** are shown in Figure 6.

The equilibrium conformer of **1a** adopts a chair conformation with the non-bonding orbitals of the O–O atoms staggered. The equatorial phenyl rings are aligned such that the π orbital of the *ipso*-carbon atom directly overlaps with the C–O bond, which through hyperconjugation allows for electronic interaction between the O–O bond and the aryl rings. The degree of this interaction may determine the stepwise character of the ET reduction mechanism. For example, in **1a** and **1b** the interaction is strong and the result is an

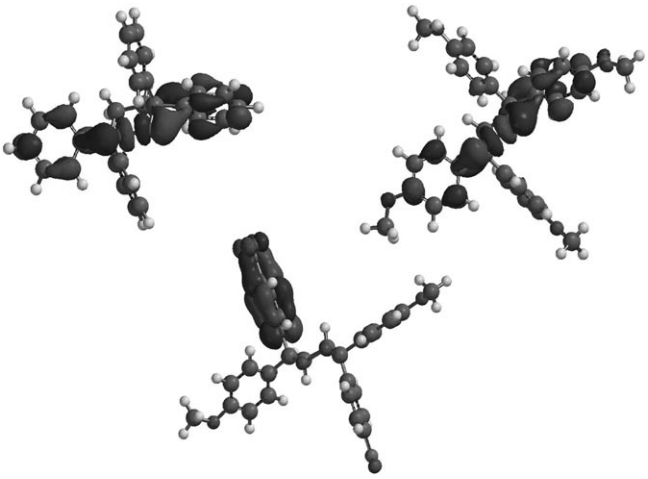

Figure 6. Depiction of the LUMOs calculated for **1a** (top left), **1b** (top right) and **1d** (bottom center).

ET reduction mechanism that falls between the concerted dissociative and stepwise dissociative mechanisms. The same calculations indicate that the π systems of the equatorial aromatic rings are not aligned perpendicular to the C–O bond in the structure of **1c**, which decreases the potential for electronic interaction between the aryl rings and O–O bond. This has important implications on the mechanism of ET, as will be discussed below.

Compound **1d** is a mixture of *cis* and *trans* isomers, and the PM3 equilibrium conformer was determined for both. Both isomers adopt a chair configuration as for **1a** and **1b**. The *trans* isomer has both of the 4-nitrophenyl rings in the axial position. This was the lowest energy conformer even when the initial structure began with both of the 4-nitrophenyl rings in the equatorial positions. One of the 4-methoxyphenyl rings is aligned for optimal overlap of the π system with the C–O bond as was seen for **1a** and **1b**, while the other is completely perpendicular with the geminal 4-nitrophenyl ring. In the *cis* isomer only one 4-nitrophenyl ring can occupy an axial position at any given time, and the 4-nitrophenyl ring that sits in the equatorial position does not align its π system with the C–O bond, while the 4-methoxyphenyl ring on the other side of the molecule does. Using these conformers the LUMO of each compound was calculated.

The LUMO for **1a** and **1b**, like the equilibrium conformers, were nearly identical and in both cases the LUMO was present on the equatorial aryl rings and spreading onto the C–O bond and across the O–O bond. Alkyl-substituted endoperoxides are considered to have the LUMO mainly associated with the O–O bond; however, this does not appear to be the case for **1a** and **1b**. Our findings support the assertion that ET occurs by a mechanism that is neither distinctly stepwise nor concerted. The singly occupied molecular orbital (SOMO) of the putative radical anion for **1a** was calculated and found to be completely localized over the O–O bond.

Although not depicted in Figure 6, the LUMO of **1c** is also delocalized over the O–O bond and the equatorial aryl rings, despite the lesser degree of overlap of the π system and the C–O bond. For **1d** the LUMO of both the *cis* and *trans* isomer are the same, being associated with an axial 4-nitrophenyl ring. This indicates that indeed the ET reduction of **1d** proceeds through a stepwise dissociative mechanism. Furthermore, the second lowest unoccupied orbital in **1d**, LUMO+1, correlates with the π system of other 4-nitrophenyl ring. Hence, with **1d** the antibonding orbital of the O–O bond is not involved in the heterogeneous ET from the electrode.

These results strengthen the argument that increasing the separation of the LUMO and the atoms of the cleaving bond increases stepwise character. While this assertion appears self-evident, the implication is that there exists species where the LUMO is not completely isolated from the cleaving bond, spatially or electronically, yet it is not localized directly over the cleaving bond either. This is the situation encountered with **1a** and **1b**, and the result is that ET occurs by a mechanism that is neither distinctly stepwise nor concerted.

Conclusions

The ET reduction of endoperoxides **1a**, **1b**, and **1c** proceeds by a mechanism that has characteristics of concerted and stepwise dissociative ET pathways. The CVs and digital simulations suggest that the heterogeneous ET is rate-determining, which is generally considered a strong indication that a concerted dissociative mechanism is in operation. The degree of stepwise character is reflected in the standard heterogeneous ET rate constant, k^{o}_{het} although the rigidity of the molecular structure also contributes to differences in k^{o}_{het}. Compound **1c** has the lowest k^{o}_{het}, which is attributed to the molecular backbone restricting the optimal conformation for ET.

The reorganization energy for the ET reduction of **1a**–**1c** is smaller than typically observed for the reduction of peroxides and endoperoxides, suggesting, with the assistance of DFT calculations, that the O–O bond does not rapidly cleave during the rate-determining step, and thus has stepwise character. The LUMO was found not to be localized on the cleaving bond, but rather distributed over the equatorial aryl rings, which contributes electron density to the O–O bond. This results in an increase in the O–O bond strength and the delocalization of the additional charge, possibility contributing to the formation of putative radical-anion species. It is suggested that separation of the LUMO from the cleaving bond increases stepwise character. This concept is evidenced by the ET reduction of **1d**. The ET reduction occurs by a stepwise dissociative mechanism as the LUMO for **1d** is primarily associated with an axial 4-nitrophenyl ring. The additional charge is initially associated with this ring prior to an intramolecular ET leading to O–O bond cleavage. This view of the ET reduction of **1d** is supported by evidence from CV, digital simulation, and DFT calculations. Collectively, the results suggest that a continuum of dissociative ET mechanisms exists for **1a**–**1d**, and that the two mechanisms do not exist solely in competition with one another. Though it was expected that the nitro-substituted analogue would proceed by a stepwise mechanism, the results suggest that a prediction of the mechanistic behavior can be made on the basis of the calculated LUMO.

Following ET and O–O bond cleavage, the distonic radical-anion species undergoes fragmentation for all TADs investigated. Furthermore, a propagating radical-anion chain mechanism is observed in all cases. The rate of fragmentation, estimated from digital simulation, is dependent on substituent. The distonic radical anions bearing electron-donating substituents fragment faster than **1d** with nitro substituents. This correlates with the basicity of the alkoxide fragment of the distonic radical anion. Furthermore, fragmentation of the distonic radical anion was observed to be at least two orders of magnitude slower than the fragmentation of the corresponding neutral biradical. The results from the

CV simulations indicate that the presence of charge can have a dramatic effect on the reactivity of a radical species. Though the charge and the spin are spatially and electronically separated, they have a combined influence on the overall reactivity. Further investigations into the reactivity of distonic radical-anions should continue to provide insight that is difficult to obtain from merely studying either the radical or anionic counterparts.

Experimental Section

The experimental details, synthesis and characterizations of the endoperoxides and products from the constant potential electrolysis studies can be found in the Supporting Information.

Acknowledgements

This work was financially supported by the Natural Sciences and Engineering Research Council of Canada (NSERC), the Government of Ontario (PREA) and the University of Western Ontario. D.L.B.S. thanks NSERC for a postgraduate scholarship. D.C.M. thanks the Ontario Government for an OGSST postgraduate scholarship. Doug Hairsine is thanked for performing the mass spectroscopic measurements.

[1] Z. V. Todres, *Organic Ion Radicals: Chemistry and Applications*, Marcel Dekker, NewYork, **2003**.
[2] L. Eberson, *Electron Transfer Reactions in Organic Chemistry*, Springer, Heidelberg, **1987**.
[3] J. P. Stevenson, W. F. Jackson, J. M. Tanko, *J. Am. Chem. Soc.* **2002**, *124*, 4271.
[4] J. M. Tanko, J. P. Phillips, *J. Am. Chem. Soc.* **1999**, *121*, 6078.
[5] M. Chahma, X. Li, P. Phillips, P. Schwartz, L. E. Brammer, Y. Wang, J. M. Tanko, *J. Phys. Chem. A* **2005**, *109*, 3372.
[6] J. M. Tanko, X. Li, M. Chahma, W. F. Jackson, J. N. Spencer, *J. Am. Chem. Soc.* **2007**, *129*, 4181.
[7] D. C. Magri, M. S. Workentin, *Org. Biomol. Chem.* **2008**, *6*, 3354.
[8] D. C. Magri, M. S. Workentin, *Chem. Eur. J.* **2008**, *14*, 1698.
[9] E. L. Clennan, C. Foote in *Organic Peroxides* (Ed.: W. Ando), Wiley, New York, **1992**.
[10] K. J. McCullough, M. Nojima, *Curr. Org. Chem.* **2001**, *5*, 601.
[11] a) D. A. Casteel, *Nat. Prod. Rep.* **1999**, *16*, 55; b) D. A. Casteel, *Nat. Prod. Rep.* **1992**, *9*, 289.
[12] a) S. R. Meshnick, T. E. Taylor, S. Kamchonwongpaisan, *Microbiol. Rev.* **1996**, *60*, 301; b) A. Robert, B. Meunier, *Chem. Soc. Rev.* **1998**, *27*, 273; c) C. W. Jefford, *Curr. Med. Chem.* **2001**, *8*, 1803; d) A. Robert, O. Dechy-Cabaret, J. Cazelles, B. Meunier, *Acc. Chem. Res.* **2002**, *35*, 167; e) P. M. O'Neill, G. H. Posner, *J. Med. Chem.* **2004**, *47*, 2945; f) P. M. O'Neill, G. H. Posner, *Acc. Chem. Res.* **2004**, *37*, 397.
[13] C. Thebtaranonth, Y. Thebtaranonth, S. Wanauppathamkul, Y. Yuthavong, *Phytochemistry* **1995**, *40*, 125.
[14] a) S. Sperry, F. A. Valeriote, T. H. Corbett, P. Crews, *J. Nat. Prod.* **1998**, *61*, 241; b) K. El Sayed, M. T. Hamann, N. E. Hashish, T. Shier, M. Kelly, A. A. Khan, *J. Nat. Prod.* **2001**, *64*, 522; c) Y.-C. Shen, C. V. S. Prakash, Y.-H. Kuo, *J. Nat. Prod.* **2001**, *64*, 324; d) D. T. A. Youssef, W. Y. Yoshida, M. Kelly, P. J. Scheuer, *J. Nat. Prod.* **2001**, *64*, 1332.
[15] M. S. Workentin, F. Maran, D. D. M. Wayner, *J. Am. Chem. Soc.* **1995**, *117*, 2120.
[16] R. L. Donkers, M. S. Workentin, *J. Phys. Chem. B* **1998**, *102*, 4061.
[17] R. L. Donkers, F. Maran, D. D. M. Wayner, M. S. Workentin, *J. Am. Chem. Soc.* **1999**, *121*, 7239.
[18] M. S. Workentin, R. L. Donkers, *J. Am. Chem. Soc.* **1998**, *120*, 2664.
[19] R. L. Donkers, M. S. Workentin, *Chem. Eur. J.* **2001**, *7*, 4012.
[20] D. C. Magri, R. L. Donkers, M. S. Workentin, *J. Photochem. Photobiol. A* **2001**, *138*, 29.
[21] D. C. Magri, M. S. Workentin, *Org. Biomol. Chem.* **2003**, *1*, 3418.
[22] R. L. Donkers, J. Tse, M. S. Workentin, *J. Chem. Soc. Chem. Commun.* **1999**, 135.
[23] R. L. Donkers, M. S. Workentin, *J. Am. Chem. Soc.* **2004**, *126*, 1688.
[24] D. L. B. Stringle, R. N. Campbell, M. S. Workentin, *J. Chem. Soc. Chem. Commun.* **2003**, 1246.
[25] F. Najjar, C. André-Barrès, C. Lacaze-Dufaure, D. C. Magri, M. S. Workentin, T. Tzèdakis, *Chem. Eur. J.* **2007**, *13*, 1174.
[26] S. Antonello, M. Musumeci, D. D. M. Wayner, F. Maran, *J. Am. Chem. Soc.* **1997**, *119*, 9541.
[27] S. Antonello, F. Maran, *J. Am. Chem. Soc.* **1997**, *119*, 12595.
[28] S. Antonello, F. Maran, *J. Am. Chem. Soc.* **1999**, *121*, 9668.
[29] S. Antonello, F. Formaggio, A. Moretto, C. Toniolo, F. Maran, *J. Am. Chem. Soc.* **2001**, *123*, 9577.
[30] S. Antonello, M. Crisma, F. Formaggio, A. Moretto, F. Taddei, C. Toniolo, F. Maran, *J. Am. Chem. Soc.* **2002**, *124*, 11503.
[31] S. Antonello, F. Formaggio, A. Moretto, C. Toniolo, F. Maran, *J. Am. Chem. Soc.* **2003**, *125*, 2874.
[32] F. Polo, S. Antonello, F. Formaggio, C. Toniolo, F. Maran, *J. Am. Chem. Soc.* **2005**, *127*, 492.
[33] R. Improta, S. Antonello, F. Formaggio, F. Maran, N. Rega, V. Barone, *J. Phys. Chem. B* **2005**, *109*, 1023.
[34] Reviews: a) J.-M. Savéant in *Advances in Physical Organic Chemistry, Vol. 26* (Ed.: D. Bethel), Academic Press, New York, **1990**, p. 1; b) J.-M. Savéant, *Acc. Chem. Res.* **1993**, *26*, 455; c) J.-M. Savéant in *Advances in Electron Transfer Chemistry, Vol. 4* (Ed.: P. S. Mariano), JAI Press, Greenwich, **1994**, p. 53; d) J.-M. Savéant in *Advances in Physical Organic Chemistry, Vol. 35* (Ed.: T. Tidwell), Academic Press, New York, **2000**, p. 117; e) C. Costentin, M. Robert, J.-M. Savéant, *Chem. Phys.* **2006**, *324*, 40; f) C. Costentin, L. Donati, M. Robert, *Chem. Eur. J.* **2009**, *15*, 785.
[35] Reviews: a) F. Maran, D. D. M. Wayner, M. S. Workentin in *Advances in Physical Organic Chemistry, Vol. 36* (Ed.: T. T. Tidwell), Academic Press, New York, **2001**, p. 85; b) S. Antonello, F. Maran, *Chem. Soc. Rev.* **2005**, *34*, 418; c) R. A. Rossi, A. B. Pierini, A. B. Penenory, *Chem. Rev.* **2003**, *103*, 71; d) A. Houmam, *Chem. Rev.* **2008**, *108*, 2180.
[36] R. K. Haynes, M. K. S. Probert, I. D. Wilmot, *Aust. J. Chem.* **1978**, *31*, 1737.
[37] K. Gollnick, A. Schnatterer, *Tetrahedron Lett.* **1984**, *25*, 185.
[38] K. Gollnick, A. Schnatterer, G. Utschick, *J. Org. Chem.* **1993**, *58*, 6049.
[39] K. Mizuno, T. Tamai, I. Hashida, Y. Otsuji, Y. Kuriyama, K. Tokumaru, *J. Org. Chem.* **1994**, *59*, 7329.
[40] In the ^{1}H NMR spectra it was noted that there were two unidentified resonances, comprising less than 10% of the product mixture. These may be due to arylmethoxy protons and aryl protons of a *p*-substituted aromatic moiety. However, the compounds were not isolated or identified.
[41] One possibility that we eluded to in references [7] and [8] is that in the presence of a weak acid, protonation of the alkoxide portion could first occur, followed by reduction of the alkoxyl portion and subsequent protonation to yield diol **3**.
[42] a) J. C. Imbeaux, J.-M. Savéant, *J. Electroanal. Chem.* **1973**, *44*, 169; b) J.-M. Savéant, D. Tessier, *J. Electroanal. Chem.* **1975**, *61*, 251.
[43] W. Adam, J. Sanabia, *J. Am. Chem. Soc.* **1977**, *99*, 2735.
[44] S. Antonello, R. Benassi, G. Gavioli, F. Taddei, F. Maran, *J. Am. Chem. Soc.* **2002**, *124*, 7529.
[45] S. Antonello, K. Daasbjerg, H. Jensen, F. Taddei, F. Maran, *J. Am. Chem. Soc.* **2003**, *125*, 14905.

Received: July 21, 2009
Published online: November 27, 2009

